Although the TNA is very general and applicable to the limit analysis of masonry structures of very complicated geometry [9], subjected to both vertical and horizontal loads [10], the evaluation of membrane stresses starting from the value of branch thrusts is troublesome. For this reason, the TNA has been recently extended to properly model membrane stresses by formulating a triangular element that substitutes branch elements of the classical thrust network model. Renamed Thrust Membrane Analysis (TMA) for obvious reasons, this new formulation takes inspiration from the extension of the FDM made by Pauletti and Pimenta [11], which proposed a force density membrane element based on a virtual work equivalence between the triangular element and the set of network branches corresponding to the element sides. Accordingly, the proposed strategy modifies assemblage and post-processing of the TNA, although the set of equilibrium equations and the solving procedures remain unchanged. Hence, all beneficial features of the TNA are inherited by the new formulation, with the additional advantage of properly modelling membrane stresses.

After illustrating the main assumptions underlying the TMA, we report on the application of the method to the limit equilibrium analysis of the domes of the Roman thermal baths of Baia (Naples). In particular, due to its interesting features, we report the case of the dome of Mercury, considered to be the prototype of the celebrated Pantheon dome in Rome.

2 Extension of the TNA to Include Membrane Elements

In this section we present an extension of the TNA that includes membrane elements within the analysis procedure formulated by Marmo and Rosati [2]. This extension is developed so as to leave unchanged the main framework of the analysis procedure. To this end, the contribution of membrane stresses is accounted for by defining a new triangular membrane element that, together with the classical branch element, is assembled to build the thrust density and the cosine director matrices employed in the standard procedure [2]. Due to space limitations we do not repeat the entire analysis procedure but, rather, we limit our description to present the contribution of each element to the equilibrium equations involved in the solving procedure. These amount to:

$$\min_{\hat{\mathbf{t}}_h} \sum \hat{\mathbf{t}}_h \text{ such that } \begin{cases} \mathbf{C}\hat{\mathbf{t}}_h = -r\mathbf{f}_h \\ \hat{\mathbf{t}}_{h,\min} \leq \hat{\mathbf{t}}_h \leq \hat{\mathbf{t}}_{h,\max} \end{cases} \tag{1}$$

and:

$$\min_{\mathbf{z},\, r} \pm r \text{ such that } \begin{cases} \mathbf{D}\mathbf{z} + \mathbf{f}_z r = \mathbf{0} \\ \mathbf{z}_{\min} \leq \mathbf{z} \leq \mathbf{z}_{\max} \\ 0 < r < +\infty \end{cases} \tag{2}$$

which correspond to horizontal and vertical equilibrium of the thrust network, respectively. The unknowns are: the components of the vector $\hat{\mathbf{t}}_h$, collecting reference thrusts associated with the branches of the network, assumed positive if compressive, and having limit values $\hat{\mathbf{t}}_{h,\min}$ and $\hat{\mathbf{t}}_{h,\max}$; the positive scalar

parameter r, described below; the vector of nodal heights $\mathbf{z}_{\max}$, whose limit values are $\mathbf{z}_{\min}$ and $\mathbf{z}_{\max}$, respectively corresponding to the intrados and extrados of the vault. Such unknowns are computed as a function of the horizontal $\mathbf{f}_h$ and vertical $\mathbf{f}_z$ nodal forces.

The parameter r plays a fundamental role. It appears both in formulas (1) and (2) and is used to select a solution corresponding to lower values of $\mathbf{z}$, i.e. shallowest or maximum thrust solution, and higher values of $\mathbf{z}$, i.e. deepest or minimum thrust solution. These two kind of solutions are obtained by selecting the signs $+$ or $-$, respectively, within the objective function of Eq. (2).

The deepest and shallowest solutions represent two limit conditions for the equilibrium of the vault. They define the range of all possible equilibrated solutions that the structure can assume. The wider this range is, the more the structure is capable to adapt to different loading conditions. In particular, the deepest and the shallowest configurations of the network are characterized by different values of r, respectively indicated by r_d and r_s. The ratio r_d/r_s is representative of the difference between the such two extremes of the set of equilibrated configurations of the thrust model.

Being $r_d > r_s$, this ratio is always greater than the unity. In particular, higher values of r_d/r_s characterize very different deepest and shallowest configurations of the network, what indicates a wide range of possible equilibrated solutions that the structure can assume. Accordingly, higher values of the ratio r_d/r_s are usually representative of safer structures. Conversely, when the ratio r_s/r_d reaches a unit value, the deepest and shallowest configurations of the network are indistinguishable; hence, a limit condition of the structure is reached.

Finally, the matrices $\mathbf{C}$ and $\mathbf{D}$ collect the cosine directors and the thrust densities of the network, respectively. They are obtained by assembling the contribution of each element of the thrust model, which in turn can be a branch or a triangular element. Details for their evaluation are given hereafter.

2.1 Branch Elements

Employed since the very first formulations of the TNA [2,6,7], the branch elements are characterized by two end nodes of position $\mathbf{x}_1$ and $\mathbf{x}_2$ and a positive reference thrust $\hat{t}_h = rt\ell_h/\ell$, where t is the branch thrust, $\ell = |\mathbf{x}_1 - \mathbf{x}_2|$ is the branch length, and ℓ_h is the projection of ℓ onto the horizontal plane. Forces $\mathbf{f}_1$ and $\mathbf{f}_2$ transmitted to end nodes are related to nodal position by:

$$\begin{pmatrix} \mathbf{f}_1 \\ \mathbf{f}_2 \end{pmatrix} = \frac{\hat{t}_h}{\ell_h} \begin{bmatrix} \mathbf{I} & -\mathbf{I} \\ -\mathbf{I} & \mathbf{I} \end{bmatrix} \begin{pmatrix} \mathbf{x}_1 \\ \mathbf{x}_2 \end{pmatrix} = \mathbf{C}^b \hat{t}_h = \mathbf{D}^b \begin{pmatrix} \mathbf{x}_1 \\ \mathbf{x}_2 \end{pmatrix} \tag{3}$$

where $\mathbf{I}$ is the second order identity tensor. The previous equation defines the cosine director matrix $\mathbf{C}^b$ and the thrust density matrix $\mathbf{D}^b$ associated with the generic branch element. These are assembled to form the matrices $\mathbf{C}$ and $\mathbf{D}$ of the entire thrust model.

2.2 Triangular Membrane Element

Triangular membrane elements are defined by the position $\mathbf{x}_1$, $\mathbf{x}_2$ and $\mathbf{x}_3$ of their three nodes and by three values of *reference thrust densities* $\hat{\mathbf{t}}^m$ associated with its sides. The Principle of Virtual Work can be used to establish an equilibrium condition that relates $\hat{\mathbf{t}}^m$ to positive semi-definite membrane thrust tensor $\boldsymbol{\tau} = (t_\xi, t_\eta, \sqrt{2}\, t_{\xi\eta})$ associated with the element, here expressed in Mandel notation. Such an equivalence yields

$$\hat{\mathbf{t}}_h^m = rA\, \boldsymbol{\Lambda}\, \mathbf{E}^{-T} \boldsymbol{\tau} \tag{4}$$

where $\hat{\mathbf{t}}_h^m$, of components $\hat{t}_{hs}^m$, $s = 1, 2, 3$, is computed as a function of: the membrane element area A; the diagonal matrix $\boldsymbol{\Lambda}$, which collects the ratios ℓ_h^s/ℓ^s along the main diagonal, ℓ^s being the length of the generic s-th side and ℓ_h^s its projection onto the horizontal plane.

The operator $\mathbf{E}$ is used to project $\boldsymbol{\tau}$ along the sides of the element. Hence it collects the products $E_{ij} = \mathbf{u}_s \cdot \mathbf{v}_j$ between the unit vectors $\mathbf{u}_s$, associated with the s-th side of the element, and the unit vector $\mathbf{v}_j$, $j = 1, 2$, of the element local reference. It is expressed in Mandel notation as:

$$\mathbf{E} = \begin{bmatrix} E_{11}^2 & E_{12}^2 & \sqrt{2}E_{11}E_{12} \\ E_{21}^2 & E_{22}^2 & \sqrt{2}E_{21}E_{22} \\ E_{31}^2 & E_{32}^2 & \sqrt{2}E_{31}E_{32} \end{bmatrix} \tag{5}$$

Forces $\mathbf{f}_1$, $\mathbf{f}_2$ and $\mathbf{f}_3$ transmitted to element nodes are related to nodal positions by:

$$\begin{pmatrix} \mathbf{f}_1 \\ \mathbf{f}_2 \\ \mathbf{f}_3 \end{pmatrix} = \begin{bmatrix} (d_2+d_3)\mathbf{I} & -d_3\mathbf{I} & -d_2\mathbf{I} \\ -d_3\mathbf{I} & (d_1+d_3)\mathbf{I} & -d_1\mathbf{I} \\ -d_2\mathbf{I} & -d_1\mathbf{I} & (d_1+d_2)\mathbf{I} \end{bmatrix} \begin{pmatrix} \mathbf{x}_1 \\ \mathbf{x}_2 \\ \mathbf{x}_3 \end{pmatrix} = \mathbf{D}^m \begin{pmatrix} \mathbf{x}_1 \\ \mathbf{x}_2 \\ \mathbf{x}_3 \end{pmatrix} \tag{6}$$

where $d_s = \hat{t}_{hs}^m/\ell_h^s$ is the so called *reference thrust density* associated with the element sides. Previous equation is used to define the thrust density matrix $\mathbf{D}^m$ of the membrane element, assembled to form the matrix $\mathbf{D}$ of the entire thrust model.

Equation (6) can be rewritten in a form that shows explicitly the dependence upon the reference thrust densities $\hat{\mathbf{t}}_h^m$, as:

$$\begin{pmatrix} \mathbf{f}_1 \\ \mathbf{f}_2 \\ \mathbf{f}_3 \end{pmatrix} = \begin{bmatrix} \mathbf{O} & \dfrac{\mathbf{x}_1 - \mathbf{x}_3}{\ell_h^{(2)}} & \dfrac{\mathbf{x}_1 - \mathbf{x}_2}{\ell_h^{(3)}} \\ \dfrac{\mathbf{x}_2 - \mathbf{x}_3}{\ell_h^{(1)}} & \mathbf{O} & \dfrac{\mathbf{x}_2 - \mathbf{x}_1}{\ell_h^{(3)}} \\ \dfrac{\mathbf{x}_3 - \mathbf{x}_2}{\ell_h^{(1)}} & \dfrac{\mathbf{x}_3 - \mathbf{x}_1}{\ell_h^{(2)}} & \mathbf{O} \end{bmatrix} \hat{\mathbf{t}}_h^m = \mathbf{C}^m \hat{\mathbf{t}}_h^m \tag{7}$$

that defines the cosine director matrix $\mathbf{C}^m$ of the triangular element, $\mathbf{O}$ being the second order null tensor.

3 The Domes of the Baia Thermal Baths: The Temple of Mercury

The domes of the archaeological complex of Baia have always fascinated scholars and travelers for the striking features of their vaulted spaces, and have been depicted in numerous works, from the medieval miniatures to the eighteenth-century engravings, up to the multitude of images that are published every day on social networks by tourists from all over the world. Among them, the one that has always aroused the greatest interest, due to its remarkable internal spatial quality and its close formal analogy with the Pantheon, is today known with the improper name of *temple of Mercury* (Fig. 1).

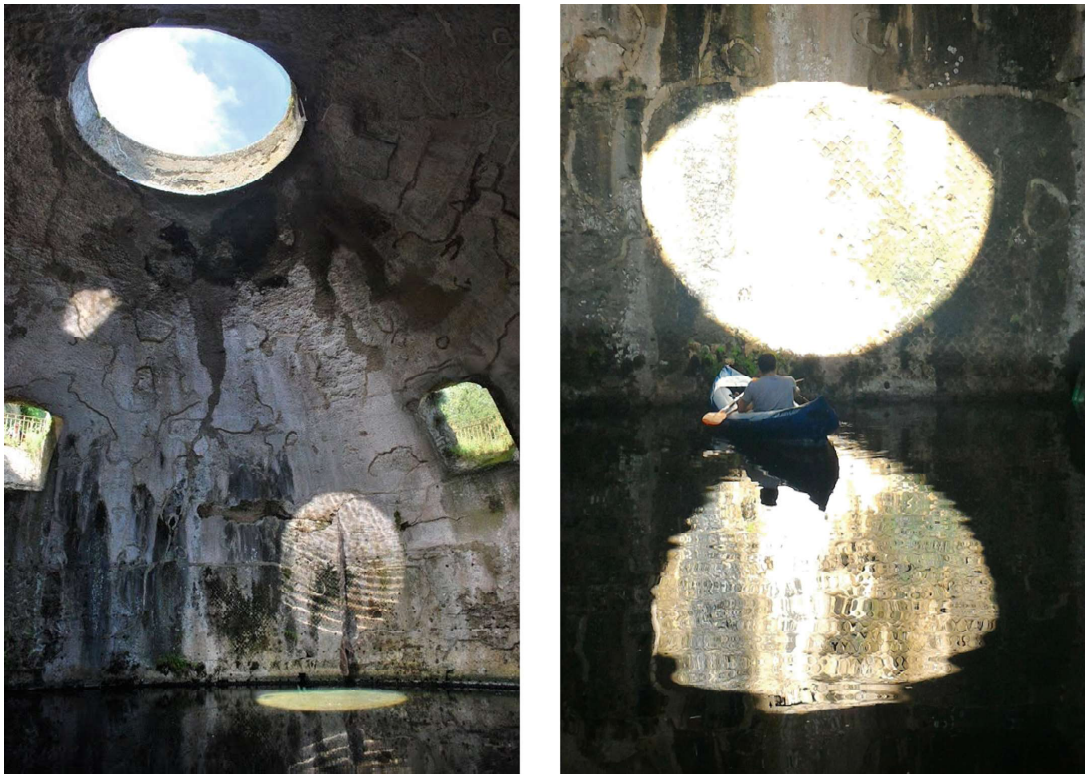

Fig. 1. Interior of the dome of Mercury and detail of the *macula* cast by the central oculus.

Built in the first century BC, the *temple of Mercury* is a frigidarium of the first imperial age, and constitutes the prototype of the most famous Roman dome. If undoubtedly it is possible to find in it an undeniable bond with the Pantheon, which is also manifested in a planned relationship between the luminous projections of the central oculus and the architectural forms of the interior spaces, there are numerous aspects that characterize it as an autonomous architectural episode and as a prototype of a technological and constructive knowledge, that in Baia developed at least until the third century AD.

3.1 Geometric, Batigraphic and Photogrammetric Survey of the Dome of Mercury

In order to construct an accurate geometric model of the dome of Mercury, a combination of geometric, batigraphic and photogrammetric survey techniques have been employed. The main difficulties in surveying this dome have been caused by the presence of water on the entire floor of the dome, with depths between 0.90 m and 1.80 m, the only exception being a small platform reachable by a steel bridge. Employing an inflatable canoe (Fig. 1 - right) it was possible to reach any point of the room, from which geometric, batigraphic and photographic data have been collected. In addition, poor light conditions increased the difficulties in shooting quality photographs from such an unstable position. This issue has been handled by shooting in manual mode and selecting the proper combination of aperture, shutter speed and ISO settings.

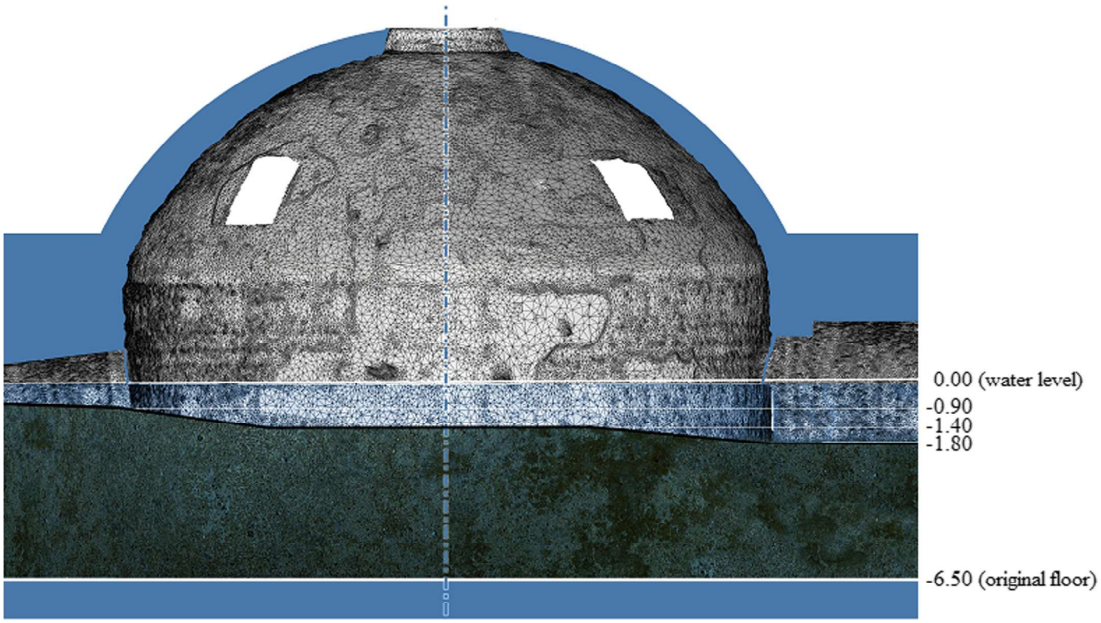

Fig. 2. Surveyed geometry of the dome of Mercury.

Figure 2 shows the result of the mentioned survey. The dome covers a circular room of diameter 21.5 m with a height of 5.7 m measured from the top of the drum to the intrados of the central oculus. The height to width ratio of this structure shows that the dome is not spherical, rather it is lowered, characterized by a polycentric meridian section. Additional 5.6 m separate the top of the drum from the water level, while 6.5 m lower is the original floor of the room, covered by water and debris.

The dome is characterized by five openings: a conic central oculus of diameter 4.45 m (at the intrados) and four rectangular windows of 1.7 m $\times$ 2.1 m, whose lower boundary is positioned at the top of the drum. It has an approximatively constant thickness of 0.75 m while the drum has variable thickness both in plan and elevation and is characterized by several recesses and openings, mostly below the water level.

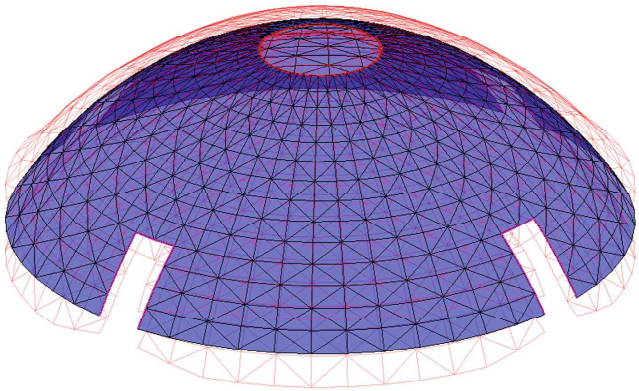

Fig. 3. Thrust model of the dome of Mercury.

3.2 Thrust Membrane Analysis of the Dome of Mercury

The thrust model of the dome has been setup by combining both branch and membrane elements. In particular, a mesh of triangular membrane elements has been used to model thrust membrane actions within the entire dome, while branch elements have been used to model the free boundaries of the five openings. Figure 3 shows the implemented thrust model, where membrane elements are represented by the blue mesh and branch elements are represented by the thicker red lines. The faint red mesh represents the limit heights of the thrust model, corresponding to the intrados and extrados of the dome.

We report the results regarding the analysis of the dome subjected to self-weight only. Nodal forces have been computed by considering the weight of concrete and tuff blocks pertaining to the relevant volume of influence of each node, assigning a weight per unit volume of 20 kN/m^3. Deepest and shallowest configurations of the thrust model have been determined by solving the optimization problems (1) and (2) and corresponding principal values of membrane thrust stresses have been computed.

Figure 4 shows the deepest configuration of the thrust network, where computed values of maximum (top) and minimum (bottom) principal thrust stresses are represented by the same colour map. As expected, this solution is characterized by a configuration that touches the intrados of the vault at the supports and the extrados in the vicinity of the central oculus. The curved geometry assumed by the perimeter of all openings show that the free boundary of the model becomes funicular of the thrust actions transmitted by interior elements. Lower values of stress above the four lateral windows show the influence of these openings on the static equilibrium of the dome.

Similar considerations can be made about the solution corresponding to the shallowest configuration of the thrust model, reported in Fig. 5. As expected, in this case, the configuration assumed by the thrust model thouches the intrados

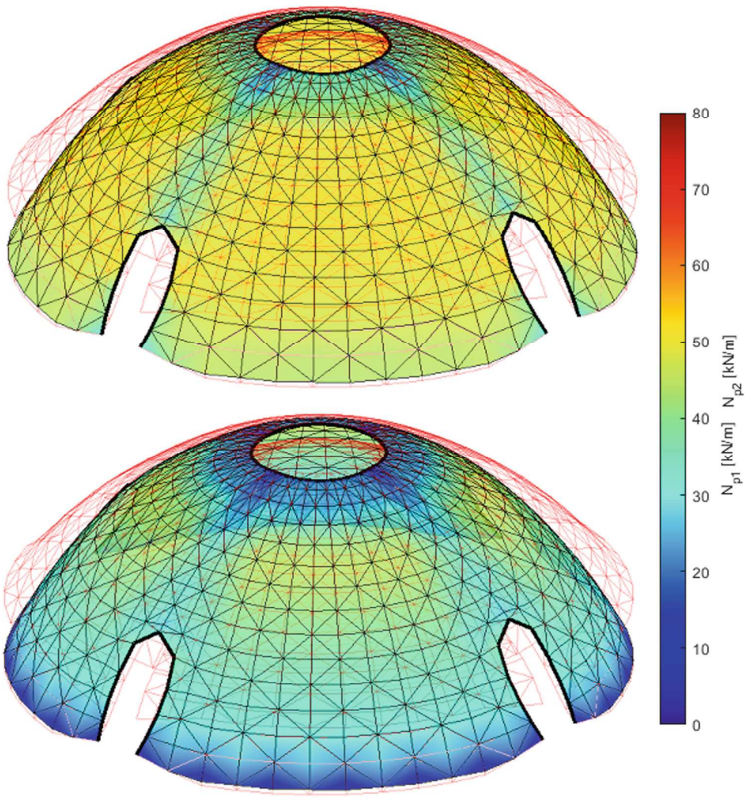

Fig. 4. Deepest configuration of the thrust model. Colours represent the computed value of the maximum (top) and minimum (bottom) principal thrust membrane stresses.

near the central oculus, and the extrados near the lateral supports. The only exception to this general rule is represented by the lower portion of the lateral openings.

The different configurations computed for the thrust membrane associated to the two solution can be appreciated by the side views of Fig. 6. From these plots it is clear how the solution of minimum thrust is characterized by a deep configuration of the thrust membrane, while the solution of maximum thrust is shallower. Here it is also clear that the solution is not axis-symmetric due to the presence of the four lateral openings.

The difference between these solutions is estimated by the ratio between the parameters r_d and r_s associated with the deepest and shallowest configurations. For the case at hand this ratio amount to $r_d/r_s \approx 1.48$, indicating a relatively high safety of this structure when subjected to vertical loads. Future analyses will focus on the analysis of the same structure subjected to both vertical and horizontal loading conditions, representative of a seismic event.

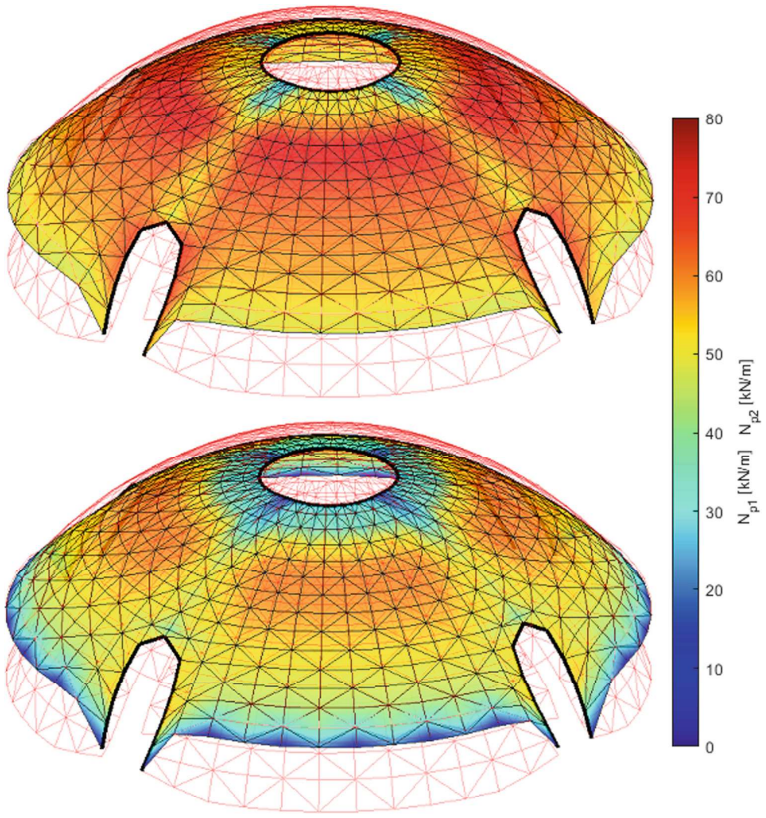

Fig. 5. Shallowest configuration of the thrust model. Colours represent the computed value of the maximum (top) and minimum (bottom) principal thrust membrane stresses.

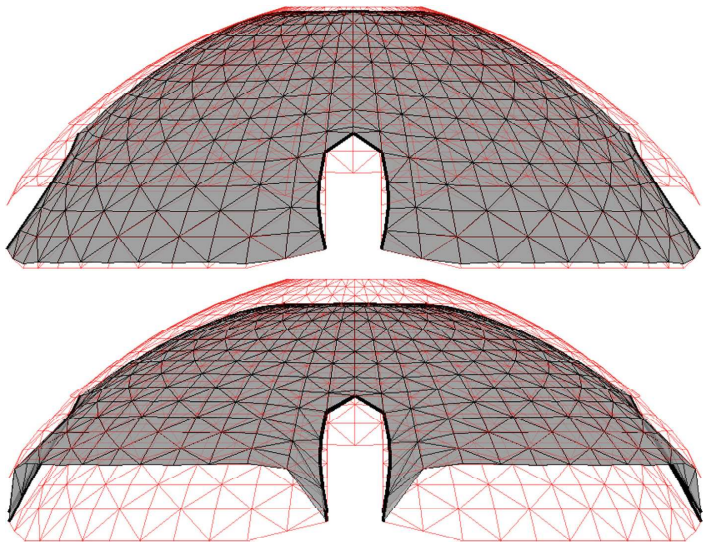

Fig. 6. Side views of the solution of minimum (top) and maximum (bottom) horizontal thrust.

4 Conclusions

We illustrated the main features of a generalization of the Thrust Network Analysis procedure that models thrust membrane actions by means of triangular elements integrated within the classical analysis procedure [2]. The proposed extension is based on a virtual work equivalence between the triangular element and the set of network branches corresponding to the element sides.

The new formulation of the TNA, renamed Thrust Membrane Analysis (TMA) for obvious reasons, has been employed to analyse the equilibrium of the oldest Roman dome still preserved to our days, the so called *temple of Mercury*, pertaining to the archaeological complex of Baia, near Naples. Although our application of the TMA is still preliminary, numerical results show the feasibility of the method.

References

1. Heyman, J.: The stone skeleton. Int. J. Solids Struct. **2**(2), 249–279 (1966)
2. Marmo, F., Rosati, L.: Reformulation and extension of the thrust network analysis. Comput. Struct. **182**, 104–118 (2017)
3. Fraternali, F.: A thrust network approach for the equilibrium problem of unreinforced masonry vaults via polyhedral stress functions. Mech. Res. Commun. **37**, 198–204 (2010)
4. Gesualdo, A., Cennamo, C., Fortunato, A., Frunzio, G., Monaco, M., Angelillo, M.: Equilibrium formulation of masonry helical stairs. Meccanica **52**(8), 1963–74 (2016)
5. Galassi, S., Misseri, G., Rovero, L., Tempesta, G.: Equilibrium analysis of masonry domes. On the analytical interpretation of the Eddy-Levy graphical method. Int. J. Archit. Herit. **11**(8), 1195–211 (2017)
6. O'Dwyer, D.: Funicular analysis of masonry vaults. Comput. Struct. **73**, 187–197 (1999)
7. Block, P., Ciblac, T., Ochsendorf, J.: Real-time limit analysis of vaulted masonry buildings. Comput. Struct. **84**(29), 1841–1852 (2006)
8. Schek, H.J.: The force density method for form finding and computation of general networks. Comput. Methods Appl. Mech. Eng. **3**, 115–134 (1974)
9. Marmo, F., Masi, D., Rosati, L.: Thrust network analysis of masonry helical staircases. Int. J. Archit. Herit. **12**, 828–848 (2018)
10. Marmo, F., Ruggieri, N., Toraldo, F., Rosati, L.: Historical study and static assessment of an innovative vaulting technique of the 19th century. Int. J. Archit. Herit. (2018). https://doi.org/10.1080/15583058.2018.1476607
11. Pauletti, R.M.O., Pimenta, P.M.: The natural force density method for the shape finding of taut structures. Comput. Methods Appl. Mech. Eng. **197**, 4419–4428 (2008)